Effects of the Molecular Weight and the Side-Chain Length on the Photovoltaic Performance of Dithienosilole/Thienopyrrolodione Copolymers

Ta-Ya Chu, Jianping Lu, Serge Beaupré, Yanguang Zhang, Jean-Rémi Pouliot, Jiayun Zhou, Ahmed Najari, Mario Leclerc,* and Ye Tao**

A series of low-bandgap alternating copolymers of dithienosilole and thienopyrrolodione (PDTSTPDs) are prepared to investigate the effects of the polymer molecular weight and the alkyl chain length of the thienopyrrole-4,6-dione (TPD) unit on the photovoltaic performance. High-molecular-weight PDTSTPD leads to a higher hole mobility, lower device series resistance, a larger fill factor, and a higher photocurrent in PDTSTPD:[6,6]-phenyl C_{71} butyric acid methyl ester ($PC_{71}BM$) bulk-heterojunction solar cells. Different side-chain lengths show a significant impact on the interchain packing between polymers and affect the blend film morphology due to different solubilities. A high power conversion efficiency of 7.5% is achieved for a solar cell with a 1.0 cm^2 active area, along with a maximum external quantum efficiency (EQE) of 63% in the red region.

1. Introduction

Organic photovoltaic (OPV) cells based on conjugated polymers have had a fast growing attraction over the past decade because of their potential as a clean and renewable energy source.[1] Recently, bulk-heterojunction (BHJ) OPV cells composed of low-bandgap polymers and [6,6]-phenyl C_{71} butyric acid methyl ester ($PC_{71}BM$) have received much attention, since the power conversion efficiency (PCE) now exceeds 7–8%,[2] demonstrating a great potential for next-generation photovoltaic devices using low-cost printing techniques for flexible PV applications. In order to improve the PCE of BHJ OPV solar cells, one strategy is to increase the open-circuit voltage (V_{oc}) of the device by increasing the energy difference between the highest occupied molecular orbital (HOMO) of the donor and the lowest unoccupied molecular orbital (LUMO) of the acceptor. For example, poly(*N*-9′-heptadecanyl-2,7-carbazole-*alt*-5,5-(4′,7′-di-2-thienyl-2′,1′,3′-benzothiadiazole)) (PCDTBT), when blended with $PC_{71}BM$, has demonstrated an efficiency of 7.1%.[2c] The energy gap (absorption) of PCDTBT (1.85 eV) is similar to that of poly(3-hexylthiophene) (P3HT) (1.90 eV); the improvement in efficiency is mainly contributed by the enhancement in V_{oc} (0.91 V) due to its deeper HOMO energy level (5.45 eV). Another strategy is to increase the short-circuit current (J_{sc}) by reducing the energy gap of the polymer to extend the absorption of the polymer/$PC_{71}BM$ blend film to a longer wavelength region. However, it remains a challenge to achieve both a high J_{sc} and a high V_{oc} in OPV cells. In the literature, most OPV cells made using low-band-gap polymers and $PC_{71}BM$ have demonstrated an increased J_{sc}, but the V_{oc} has remained low (≈0.7 V) because of the high-lying HOMO energy levels of the polymers. Recently, we reported a promising copolymer of 4,4-bis(2-ethylhexyl)-dithieno[3,2-b:2′,3′-d]silole and *N*-octylthieno[3,4-c] pyrrole-4,6-dione (PDTSTPD-C8), which possesses both a low optical energy gap (1.73 eV) and a deep HOMO energy level (5.57 eV). A high V_{oc} (≈0.9 V) and a high J_{sc} (≈12 mA cm^{-2}, the absorption covers a broad wavelength range from 300 nm to 690 nm) have been demonstrated for OPV cells using $PC_{71}BM$ as the electron acceptor.[2d]

In addition to the chemical structures of the donor and acceptor materials, the control of the nanoscale morphology of the OPV active layer has been a focus of intense study, in order to have efficient exciton dissociation and charge collection. Various strategies have been used in OPV cell fabrication to form nanoscale, interpenetrating, bicontinuous networks of a conjugated polymer (donor) and fullerene derivative (acceptor). Thermal annealing[3] and a slow growth[4] process have been used for regioregular *rr*-P3HT-based OPV-cell fabrication. The improved P3HT crystallinity led to enhancement in both the photoabsorption and the hole mobility. More recently, significant progress has been made by using mixed solvents or processing additives for amorphous copolymers and fullerene BHJ films.[5] In this work, we synthesized a series of dithienosilole/thienopyrrolodione copolymers (PDTSTPDs) with different alkyl chain lengths in the thienopyrrole-4,6-dione (TPD) unit with the aim of enhancing the interchain interaction and

Dr. T.-Y. Chu, Dr. J. Lu, Dr. Y. Zhang, J. Zhou, Dr. Y. Tao
Institute for Microstructural Sciences (IMS)
National Research Council of Canada (NRC)
Ottawa, ON, K1A 0R6, Canada
E-mail: Jianping.Lu@nrc.ca; Ye.Tao@nrc.ca
Dr. S. Beaupré, J.-R. Pouliot, Dr. A. Najari,
Prof. M. Leclerc
Département de Chimie
Université Laval
Quebec City, QC, G1V 0A6, Canada
Email: Mario.Leclerc@chm.ulaval.ca

DOI: 10.1002/adfm.201102623

fine-tuning the polymer solubility. We also investigated the effects of the molecular weight and the side-chain lengths of PDTSTPDs on the blend film morphology and OPV performance. A power conversion efficiency as high as 7.5% was achieved for solar cells with an active area of 1.0 cm^2, which is among the best performances to date.

2. Results and Discussion

2.1. Molecular Weight Effect

The molecular weight of *rr*-P3HT has a significant impact on the resulting film morphology and hole mobility. High-molecular-weight *rr*-P3HT has demonstrated three orders of magnitude improvement in hole mobility, and a much enhanced OPV cell efficiency.[6] However, some conjugated polymers have a relatively poor solubility in organic solvents when their molecular weights are high, and thus require the polymer/$PC_{71}BM$ blend films to be deposited from a hot solution.[7] It is well known that the introduction of branched alkyl or alkoxy side chains can improve the solubility of high-molecular-weight polymers.[8] We used two ethylhexyl groups on the dithienosilole unit to improve the solubility, and prepared a series of PDTSTPD-C8 copolymers with number-average molecular weights of 10 kDa, 18 kDa and 31 kDa. These three PDTSTPDs-C8 of different molecular weights were obtained by Soxhlet extraction using different solvents. The 10 kDa fraction was extracted with hot hexanes, the 18 kDa fraction with dichloromethane, and the 31 kDa part with chloroform. Therefore, these three polymers had very different solubilities in organic solvents; the higher molecular weight polymer had lower solubility. It is well-known that the optical bandgaps of organic semiconductors decrease on increasing the conjugation lengths.[9] However, when an effective conjugated length for the energy gap is reached, the bandgap does not change any more. The absorption maxima (λ_{max}) of PDTSTPDs-C8 of M_n = 18 kDa and 31 kDa were almost the same, indicating that the effective conjugation length for the optical bandgap of PDTSTPD-C8 is below 18 kDa. However, the film absorption coefficient continued to increase slightly when the polymer molecular weight increased from 18 to 31 kDa. The low-molecular-weight fraction (10 kDa) had a slightly larger optical energy gap, with a 6 nm blue-shift in the absorption maximum, as shown in **Figure 1**. In addition, its film absorption coefficient was the lowest among the three fractions. A PCE of 3.1% was obtained with the low-molecular-weight PDTSTPD-C8, which is similar to the result (2.13%) published by Zhang et al. from the same polymer with a molecular weight of 13.6 kDa.[10] A significant improvement in the PV performance was observed with the high-molecular-weight PDTSTPDs, as shown in **Figure 2**. The PCE was improved to 5.4% and 7.7% when the molecular weight was increased to 18 kDa and 31 kDa, respectively. The measured parameters of the OPV performance are shown in **Table 1**. There is less than 4% deviation in J_{sc} between the solar simulator and the external quantum efficiency (EQE) measurements. The EQE-calibrated PCE reached 7.5% for devices fabricated from the 31 kDa PDTSTPD-C8. The EQE spectra of the OPV devices made from the PDTSTPDs of different molecular

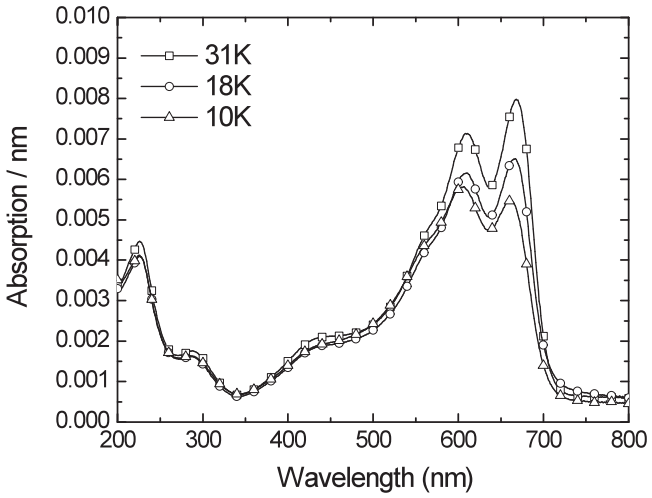

Figure 1. Absorption spectra (normalized by the film thickness) of the spin-cast PDTSTPD-C8 films of different molecular weights.

weights showed significant improvement across the whole photoresponse region, with increasing polymer molecular weight, indicating that the enhancement in J_{sc} was mainly due to more efficient exciton dissociation and charge collection from both the PDTSTPD and the $PC_{71}BM$ domains with increasing polymer molecular weight.

Figure 3 shows the *I–V* curves of bottom-contact field-effect transistors (FETs) at different gate voltages for the PDTSTPD-C8 of different molecular weights. The carrier mobility and the film morphology are two major factors that could be significantly affected by the polymer molecular weight. When the molecular weight increased from 10 kDa to 18 kDa and 31 kDa, the hole mobility of the PDTSTPD-C8 increased from 7×10^{-6} to 1×10^{-4} and 3.7×10^{-4} cm^2 V^{-1} s^{-1}. There was a difference about two orders of magnitude in mobility between the 10 kDa and 31 kDa PDTSTPD-C8. The OPV cells made with high-molecular-weight PDTSTPD-C8 not only had a higher J_{sc}, but also exhibited a higher fill factor (FF), as shown in Table 1. The enhanced FF is attributed to the relatively low series resistance of the cells due to the high hole mobility of the high-molecular-weight PDTSTPD-C8. The series resistance of the OPV cells decreased from 9 to 5 Ω cm^2 when the molecular weight of the polymer increased from 10 kDa to 31 kDa.

In addition, the enhanced OPV performance was not only due to the increased carrier mobility, but also due to the improved nanoscale morphology of the BHJ film. As compared with the change in hole mobility between the 18 kDa and 31 kDa polymers, the improvement in PCE was much more significant (more than 40%). The improvement in mobility alone cannot fully explain the ≈40% gain in PCE. Through an atomic force microscopy (AFM) study, we could reasonably attribute the PCE gain partly to the improved nanoscale morphology of the interpenetrating PDTSTPD-C8/$PC_{71}BM$ network with increasing polymer molecular weight. An ideal interpenetrating network would provide a large interface between the polymer and the $PC_{71}BM$, allowing efficient exciton dissociation, and also presenting a bicontinuous network that would enhance charge transport with low recombination. A discontinuous network will result in a reduction in charge-collection efficiency,

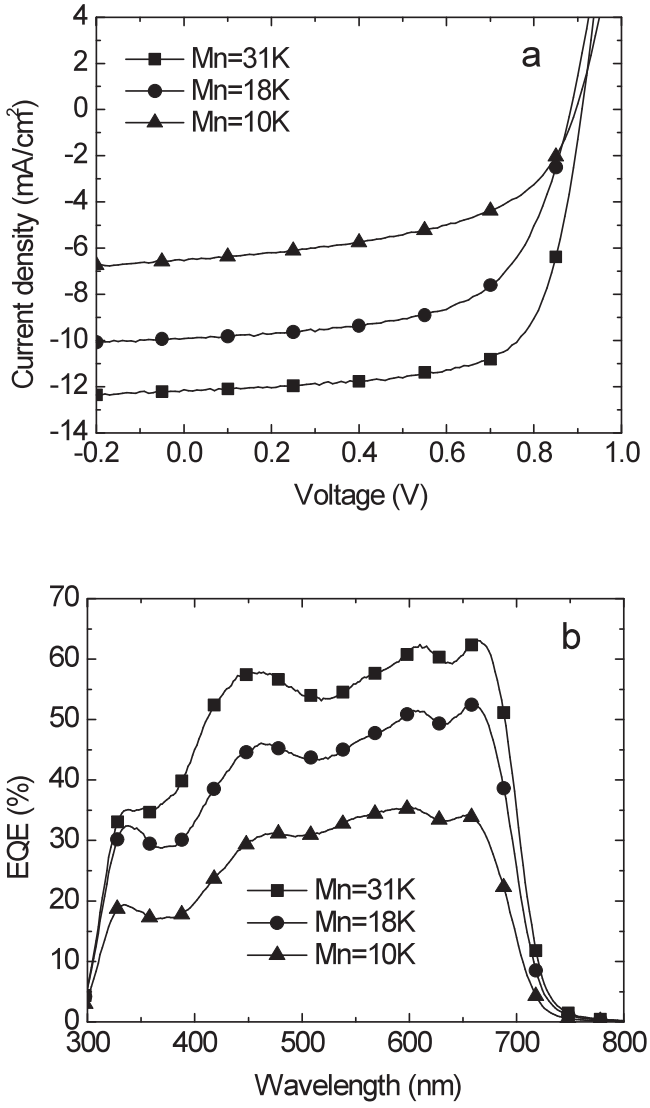

Figure 2. a) Current density–voltage characteristics of the solar cells fabricated with different molecular weight PDTSTPD-C8 blended with $PC_{71}BM$, measured under AM 1.5G illumination. b) EQE spectra of the solar cells for the different molecular weight PDTSTPD-C8 blended with $PC_{71}BM$.

leading to a lower J_{sc} and FF. It is well-known that the relative solubility of the polymer to the fullerene derivative in the processing solvent greatly affects the final film morphology.

Table 1. Photovoltaic parameters of PDTSTPD-C8:$PC_{71}BM$ - based solar cells fabricated with different molecular weights.

M_n [kDa]	PCE [%]	J_{sc} [mA cm^{-2}]	V_{oc} [V]	FF [%]	EQE J_{sc} [mA cm^{-2}]	Calibrated PCE [%]	R_{sh} [kΩ]	R_s [Ω]
31	7.7	−12.13	0.910	70	11.8	7.5	1.5	5
18	5.4	−9.91	0.884	62	9.5	5.2	1.3	7
10	3.1	−6.53	0.896	53	6.3	3.0	0.8	9

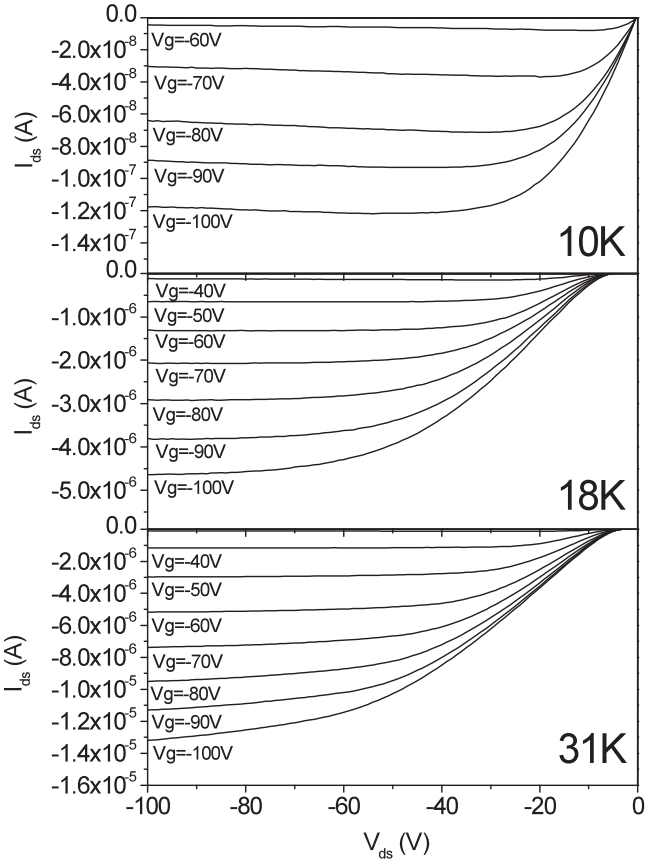

Figure 3. Source-drain *I–V* curves of the bottom contact OFETs for the different-molecular-weight PDTSTPD-C8 films.

When the PDTSTPD-C8/$PC_{71}BM$ blend film was prepared without 1,8-di-iodo-octane (DIO), fullerene precipitated out first to form large, isolated aggregates (about 0.5 μm in diameter), as confirmed by Auger electron spectroscopy (AES) sulfur and carbon mapping images (see **Figure 4**). $PC_{71}BM$ does not contain S atoms, but has a high C content. The presence of the dark spots in the AES S mapping image and the bright spots in the C mapping image proved unambiguously the formation of large $PC_{71}BM$ aggregates when the blend film was prepared without DIO. Since DIO selectively dissolves fullerene, the use of a DIO additive could increase the relative solubility of the fullerene to the polymer in the processing solution, to ensure that the two materials could come out at the same time during the spin-casting process. As a result, the AES sulfur and carbon mapping images showed a uniform distribution of both S and C elements in the blend film prepared with DIO. **Figure 5** shows AFM images of the blend films (prepared from the CB + 3% DIO solution). It is interesting to point out that the PDTSTPD-C8/$PC_{71}BM$ blend films using polymers of different molecular weight presented similar height images with root-mean-square roughnesses of about 7 nm, but the phase images showed a clear difference at the 500 nm scan scales. The blend film prepared with low-molecular-weight (10 kDa) PDTSTPD-C8 and $PC_{71}BM$ showed a clear, phase-separated morphology with finer, fibrous nanoscale domains. When the polymer molecular weight increased, its solubility decreased and it tended to form

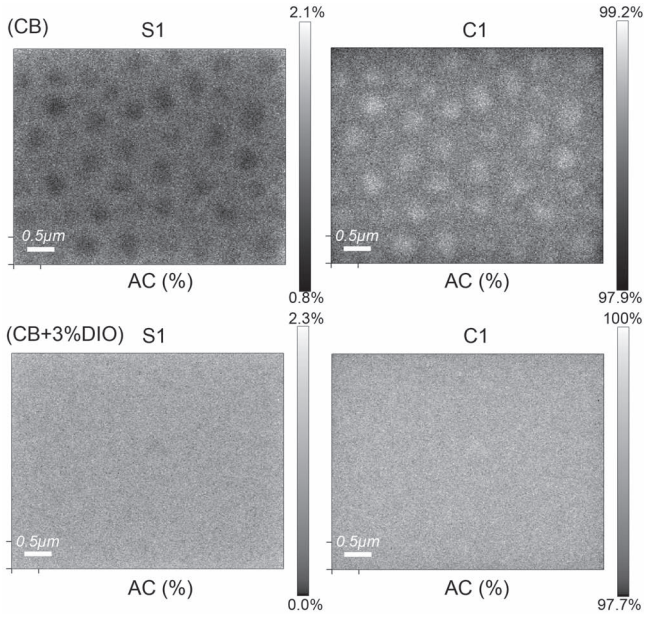

Figure 4. Auger electron spectroscopy (AES) sulfur and carbon mapping images for the PDTSTPD-C8:$PC_{71}BM$ blend films prepared from CB solution with and without DIO.

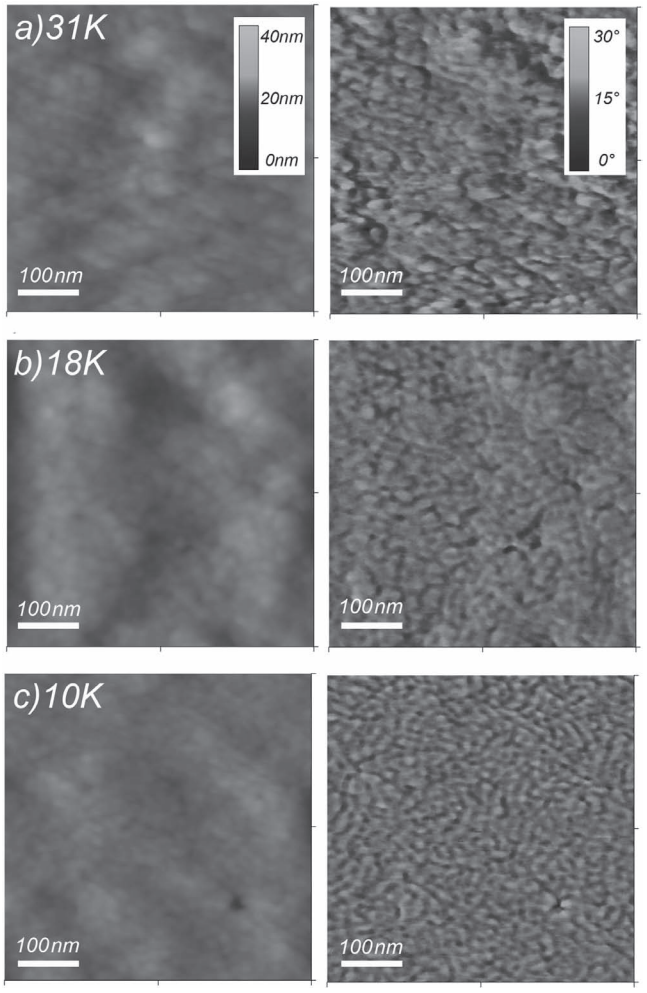

Figure 5. AFM height (left) and phase (right) images of the different molecular weight PDTSTPD-C8 and $PC_{71}BM$ blend films (prepared from the solutions CB + 3% DIO).

aggregates. As a result, the domain size became larger (≈20 nm in width, still comparable to the exciton diffusion length) and, meanwhile, less discontinuous phase separation was observed. From the above observations, we conclude that the polymer molecular weight significantly influences the PV performance via its impact on both the the active layer morphology and the charge mobility.

2.2. Different Alkyl Chain Lengths in the Thienopyrrolodione Unit

As pointed out in the study on the molecular weight effect, the relative solubility of the polymer to the $PC_{71}BM$ had a significant impact on the final morphology of the active layer. With an attempt to enhance the interchain interaction and to fine-tune the polymer solubility, we shortened the alkyl chain lengths in the thienopyrrole-4,6-dione (TPD) unit from C8 to C6 and C4, as shown in **Scheme 1**. After purification by Soxhlet extraction with hexanes, dichloromethane, and chloroform, the molecular weights of the purified PDTSTPD-C6 and PDTSTPD-C4 were 26 and 25 kDa, respectively. DSC analysis showed that the glass transition temperatures of these three polymers were similar, all around 109 °C. Interestingly, they also had similar hole mobilities, around 2–4 × 10^{-4} cm^2 V^{-1} s^{-1}, as measured from bottom-contact field-effect transistors (FET) on SiO_2/Si substrates. X-ray diffraction measurements of the three polymer films spin-cast at room temperature all revealed a π–π stacking with a similar *d*-spacing of ≈4.2 Å. However, to our surprise, only PDTSTPD-C8 could form a lamellar structure with an additional diffraction peak at $2\theta \approx 4.6°$, corresponding to a *d*-spacing of ≈19.3 Å, as shown in **Figure 6**. This implies a better polymer-chain organization in the PDTSTPD-C8 film.

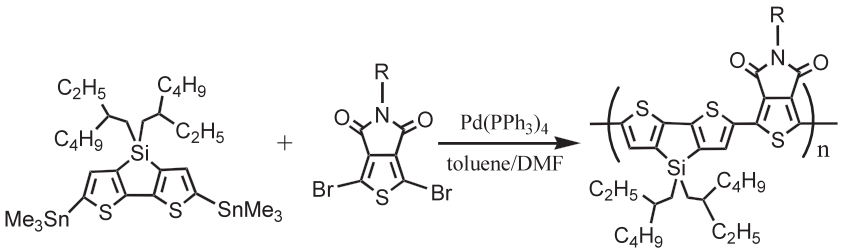

PDTSTPD-C8: R = C_8H_{17}
PDTSTPD-C6: R = C_6H_{13}
PDTSTPD-C4: R = C_4H_9

Scheme 1. Synthesis of the PDTSTPD copolymers.

Although these three polymers had similar glass transition temperatures, their

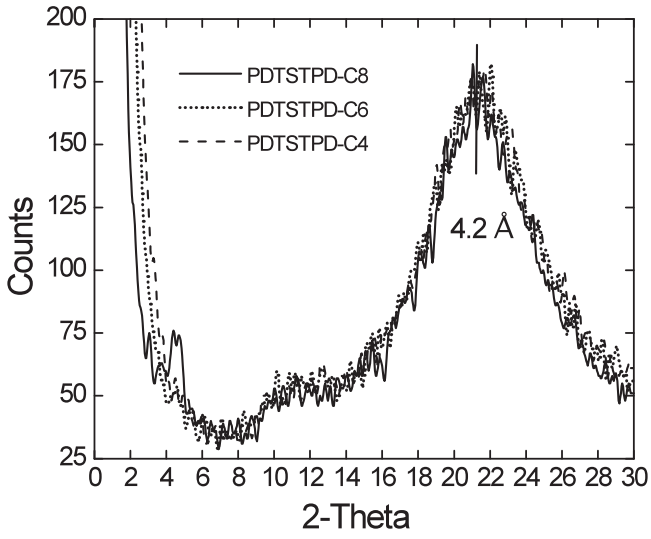

Figure 6. X-ray diffraction patterns for the different side-chain length PDTSTPD films. PDTSTPD-C8 shows an additional diffraction peak at $2\theta \approx 4.6°$, indicating the formation of lamellar structures in the film.

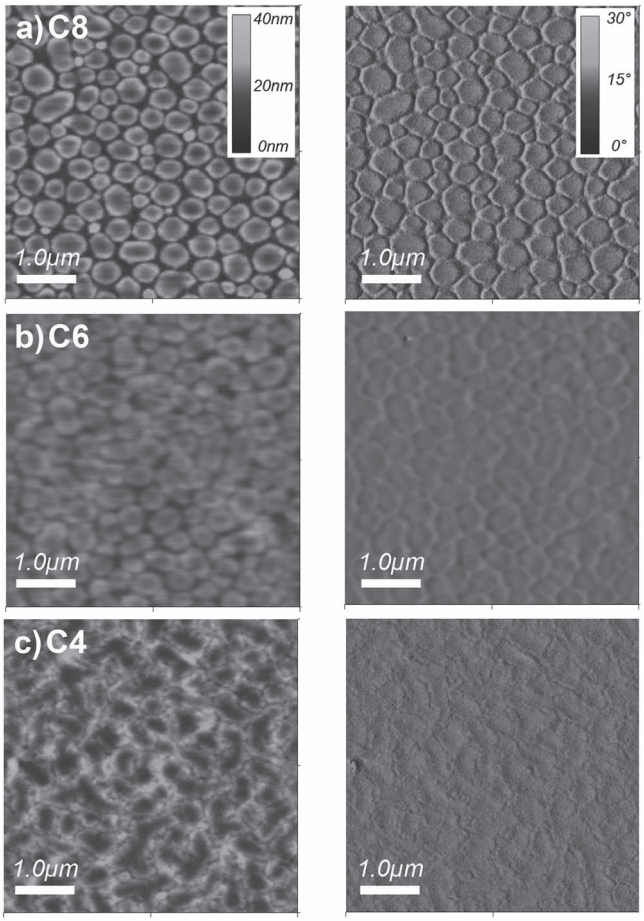

Figure 7. AFM height (left) and phase (right) images of the PDTSTPD-C8, PDTSTPD-C6 and PDTSTPD-C4 blended with $PC_{71}BM$ prepared without processing additive.

solubilities in organic solvents were very different. The solubility decreased monotonously on shortening the alkyl chain length in the TPD unit from C8 to C6 and C4. For instance, it was difficult to dissolve PDTSTPD-C4 completely in chlorobenzene (CB) at room temperature. Therefore, 1,2-dichlorobenzene (o-DCB) was chosen as a solvent. As mentioned in the polymer molecular weight study, large, island-like $PC_{71}BM$ clusters were observed when the PDTSTPD-C8/$PC_{71}BM$ blend film was prepared without DIO. This kind of morphology causes inefficient exciton dissociation and charge collection. As a result, a very low efficiency of 0.9% was obtained for the devices fabricated without DIO. It is interesting to note that we observed a totally different morphology in the PDTSTPD-C4/$PC_{71}BM$ blend film. In contrast to the formation of the large, isolated $PC_{71}BM$ clusters, a morphology with a continuous $PC_{71}BM$ phase was observed, even when the PDTSTPD-C4/$PC_{71}BM$ blend film was prepared without the use of any processing additives, as shown in **Figure 7**. An efficiency of 2.5% was achieved, which is much higher than the value of 0.9% for the PDTSTPD-C8-based solar cell fabricated under the same conditions. It is clear that the reduction of the polymer solubility favors the formation of an interpenetrating donor-acceptor network, which has a similar effect to the approach using DIO additive, to increase the solubility of $PC_{71}BM$ and meanwhile decrease the solubility of polymer. It all comes to tuning the relative solubilities of the two components in a system to achieve an optimized relative precipitation rate. The PV performance parameters of PDTSTPD-C4 and PDTSTPD-C6 are summarized in **Table 2**. The efficiency of the PV cells based on PDTSTPD-C4 increased to 5.1% when 1% DIO was used as a processing additive. However, a higher DIO concentration (>2% by volume) produced large (visible by naked eyes) PDTSTPD-C4 particles in the spin-cast blend films, leading to a poor device performance. For the PDTSTPD-C6/$PC_{71}BM$ system, the optimized DIO concentration was 2% (by volume). An EQE-calibrated PCE of 6.3%

Table 2. Photovoltaic parameters of the solar cells based on PDTSTPD-C4:$PC_{71}BM$ and PDTSTPD-C6:$PC_{71}BM$ BHJ films prepared under different conditions.

	PCE [%]	J_{sc} [mA cm^{-2}]	V_{oc} [V]	FF [%]	EQE J_{sc} [mA cm^{-2}]	Calibrated PCE [%]	R_{sh} [kΩ]	R_s [Ω]
C4 (o-DCB)	2.4	−5.20	0.86	55	5.3	2.5	0.7	4
C4 (o-DCB + 1% DIO)	5.3	−9.65	0.90	61	9.2	5.1	0.7	5
C6 (CB + 2% DIO)	5.7	−10.43	0.88	62	10.0	5.5	1.2	5
C6 (o-DCB + 2% DIO)	6.4	−10.91	0.90	65	10.8	6.3	0.7	6

was obtained when the BHJ film was spin-cast from an o-DCB solution with 2% DIO. A relatively lower efficiency of 5.5% was obtained when PDTSTPD-C6/$PC_{71}BM$ was spin-cast from a CB solution with 2% DIO. Therefore, the optimized concentration of the processing additive depends strongly on the polymer solubility and the thin-film preparation process.

3. Conclusions

In summary, we have investigated the effects of the polymer molecular weight and the alkyl chain length of the thienopyrrole-4,6-dione (TPD) unit in PDTSTPD on the photovoltaic performance. High-molecular-weight PDTSTPD is required for photovoltaic applications because of the associated high mobility in the polymer. The fill factor was increased to 70% when using high-molecular-weight PDTSTPD (31 kDa), due to the decreased series resistance. We found that longer alkyl chains (C_8H_{17}) in the TPD unit not only improved the polymer solubility, but also facilitated the formation of lamellar structures in the spin-cast films and the length of the alkyl side chains had a significant impact on the morphology when the PDTSTPD was blended with $PC_{71}BM$. A power conversion efficiency of 7.5% was demonstrated for solar cells with an active area of 1.0 cm^2 after the optimization of both materials and the device fabrication process.

4. Experimental Section

Polymer Synthesis: 4,4-bis(2-ethylhexyl)-2,6-bis(trimethyltin)-dithieno[3,2-*b*:2′,3′-*d*]silole (1.05 equiv.) and 1,3-dibromo-5-alkylthieno[3,4-*c*] pyrrole-4,6-dione (1 equiv were added to a 50 mL oven-dried one-necked flask. The flask was purged 3 times with argon, and then tetrakis(triphenylphosphine)palladium(0) ($Pd(PPh_3)_4$) (0.08 equiv.) was added in a nitrogen-filled glove-box. Degassed toluene/*N*,*N*-dimethylformamide (DMF) (10:1, v/v) was added under an argon atmosphere, and the resulting solution was stirred at 115 °C under argon. After 42 h of polymerization, trimethylphenyltin (0.15 equiv.) in 0.75 mL of degassed toluene/DMF (10:1, v/v) was added to the reaction flask and the reaction was kept at 115 °C for an additional 5 h. Bromobenzene (0.5 equiv.) in 0.75 mL of degassed toluene/DMF (10:1, v/v) was then added to the reaction flask, and the temperature was kept at 110 °C for an additional 8 h to complete the end-capping reaction. The dark-blue polymerization solution was cooled to room temperature and precipitated in methanol. The resultant polymer was collected by filtration, dried and extracted successively with hexanes and dichloromethane using a Soxhlet extraction apparatus. The remaining solid was extracted with 200 mL of chloroform. After evaporation of the chloroform under reduced pressure, methanol was added and the polymer film, with a metal lustre, was collected by filtration. PDTSTPD-C8: Yield 46%; M_n = 31 kDa and PDI = 1.58; ^{1}H NMR (400 MHz, 1,2-dichlorobenzene-d_4, 50 °C, δ) 8.74 (s, 1H), 7.68 (s, 1H), 3.80 (br, 2H), 2.40–0.40 (m, 49H). Anal. calcd for $C_{38}H_{53}NO_2S_3Si$: C 67.11, H 7.86, N 2.06, O 4.70, S 14.14, Si 4.13; found: C 66.65, H 7.85, N 2.39. PDTSTPD-C6: Yield 48%. M_n = 26 kDa and PDI = 1.63; ^{1}H NMR (400 MHz, 1,2-dichlorobenzene-d_4, 50 °C, δ): 8.72 (s, 1H), 7.65 (s, 1H), 3.77 (br, 2H), 2.40–0.40 (m, 45H); Anal. calcd for $C_{36}H_{49}NO_2S_3Si$: C 66.31, H 7.57, N 2.15, O 4.91, S 14.75, Si 4.31; found: C 65.68, H 7.50, N 2.22. PDTSTPD-C4: Yield 51%; M_n = 25 kDa and PDI = 1.62; ^{1}H NMR (400 MHz, 1,2-dichlorobenzene-d_4, 50 °C, δ): 8.72 (s, 1H), 7.66 (s, 1H), 3.78 (br, 2H), 2.40–0.40 (m, 41H); Anal. calcd for $C_{34}H_{45}NO_2S_3Si$: C 65.44, H 7.27, N 2.24; O 5.13, S 15.42, Si 4.50; found: C 65.18, H 7.25, N 2.24.

FET Mobility Measurements: The hole mobilities of the polymers were measured using organic field-effect transistors (OFETs) with a bottom-contact structure. Gold source and drain electrodes were sputtered on a SiO_2/Si substrate prior to the deposition of the polymer film. The channel widths and the lengths of the transistors were 10 mm and 20 μm, respectively. The polymer thin films were spin-coated on the SiO_2/Si substrates from chlorobenzene solutions to cover the source and drain electrodes. The OFETs were characterized inside a dark box at room temperature and under nitrogen using an Agilent (4155c) semiconductor parameter analyzer. The hole mobilities were calculated in the saturation regime at V_{DS} = –100 V using Equation 1:

$$I_{DS} = \left(\frac{W}{2L}\right) \mu C_i (V_G - V_T)^2 \quad (1)$$

where V_{DS} is the source-drain voltage, I_{DS} is the source-drain current, W and L are, respectively, the channel width and length, μ is the field-effect mobility, C_i is the capacitance per unit area of the SiO_2 layer, and V_G and V_T are, respectively, the gate voltage and threshold voltage.

Fabrication and Characterization of Organic Solar Cells: The BHJ solar cells were prepared on commercial glass slides coated with patterned indium tin oxide (ITO). The thickness and sheet resistance of the ITO were 90 nm and 18 Ω per square, respectively. The active area of each solar-cell device was 1.0 cm^2, with a length:width ratio of 4:1. The substrates were sonicated sequentially in acetone, and isopropyl alcohol. Immediately prior to the device fabrication, the substrates were treated in a UV-ozone oven for 15 min. Firstly, a poly(3,4-ethylenedioxythiophene)-poly(styrene sulfonate) (PEDOT-PSS) thin film (30 nm) was spin-coated at 9000 rpm and then baked at 140 °C for 15 min. Secondly, an active layer (90 nm) was spin-coated on top of the PEDOT-PSS from solutions of the polymer:PC71BM blends with a weight ratio of 1:2. In the case of the devices using a processing additive, 1,8-di-iodo-octane (1–3% by volume) was added to the solutions before use. Finally, 5 nm of bathocuproin (BCP) and 80 nm of Al were deposited on the top of the active layer under a vacuum of 8×10^{-7} Torr to complete the PV device fabrication. The solar cells (with no protective encapsulation) were then tested in air under an AM 1.5G illumination of 100 mW cm^{-2} (ScienceTech Inc., SS 500W solar simulator) calibrated with a KG5-filter-covered silicon photovoltaic solar cell. The current–voltage (*I*–*V*) characteristics were recorded using a computer-controlled Keithley 2400 source meter. The EQE measurements were performed using a Jobin–Yvon Triax spectrometer, a Jobin–Yvon xenon light source, a Merlin lock-in amplifier, a calibrated Si UV detector and an SR570 low-noise current amplifier.

Acknowledgements

Financial support from Sustainable Development Technology Canada (SDTC) is greatly acknowledged. The authors also thank Mr. Oltion Kodra and Mr. Terry Quance at NRC for their technical support, and Dr. Reda Aich at Université Laval for helpful discussion. The government of Canada owns the Crown copyright for this article.

Received: October 31, 2011
Revised: January 19, 2012
Published online: March 6, 2012

[1] a) G. Yu, J. Gao, J. C. Hummelen, F. Wudl, A. J. Heeger, *Science* **1995**, *270*, 1789; b) B. C. Thompson, J. M. J. Fréchet, *Angew. Chem. Int. Ed.* **2008**, *47*, 58; c) J. Peet, A. J. Heeger, G. C. Bazan, *Acc. Chem. Res.* **2009**, *42*, 1700; d) G. Dennler, M. C. Scharber, C. J. Brabec, *Adv. Mater.* **2009**, *21*, 1323; e) D. Mühlbacher, M. Scharber, M. Morana, Z. Zhu, D. Waller, R. Gaudiana, C. Brabec, *Adv. Mater.* **2006**, *18*, 2884.

[2] a) H.-Y. Chen, J. Hou, S. Zhang, Y. Liang, G. Yang, Y. Yang, L. Yu, G. Li, *Nat. Photonics* **2009**, *3*, 649; b) Y. Liang, Z. Xu, J. Xia, S. Tsai,

Y. Wu, G. Li, C. Ray, L. Yu, *Adv. Mater.* **2010**, *22*, E135; c) T.-Y. Chu, S. Alem, S-W. Tsang, S.-C. Tse, S. Wakim, J. Lu, G. Dennler, D. Waller, R. Gaudiana, Y. Tao, *Appl. Phys. Lett.* **2011**, *98*, 253301; d) T.-Y. Chu, J. Lu, S. Beaupré, Y. Zhang, J.-R. Pouliot, S. Wakim, J. Zhou, M. Leclerc, Z. Li, J. Ding, Y. Tao, *J. Am. Chem. Soc.* **2011**, *133*, 4250; e) C. M. Amb, S. Chen, K. R. Graham, J. Subbiah, C. E. Small, F. So, J. R. Reynolds, *J. Am. Chem. Soc.* **2011**, *133*, 10062; f) Z. He, C. Zhong, X. Huang, W. Wong, H. Wu, L. Chen, S. Su, Y. Cao, *Adv. Mater.* **2011**, *23*, 4636.

[3] a) W. L. Ma, C. Y. Yang, X. Gong, K. Lee, A. J. Hegger, *Adv. Funct. Mater.* **2005**, *15*, 1617; b) L. Zeng, C. W. Tang, S. H. Chen, *Appl. Phys. Lett.* **2010**, *97*, 053305; c) R. A. Marsh, J. M. Hodgkiss, S. Albert-Seifried, R. H. Friend, *Nano Lett.* **2010**, *10*, 923.

[4] a) G. Li, V. Shrotriya, J. Huang, Y. Yao, T. Moriarty, K. Emery, Y. Yang, *Nat. Mater.* **2005**, *4*, 864; b) P. G. Karagiannidis, D. Georgiou, C. Pitsalidis, A. Laskarakis, S. Logothetidis, *Mater. Chem. Phys.* **2011**, *129*, 1207.

[5] a) J. Peet, C. Soci, R. C. Coffin, T. Q. Nguyen, A. Mikhailovsky, D. Moses, G. C. Bazan, *Appl. Phys. Lett.* **2006**, *89*, 252105; b) J. Peet, J. Y. Kim, N. E. Coates, W. L. Ma, D. Moses, A. J. Heeger, G. C. Bazan, *Nat. Mater.* **2007**, *6*, 497; c) F. Zhang, K. G. Jespersen, C. Björström, M. Svensson, M. R. Andersson, V. Sundström, K. Magnusson, E. Moons, A. Yartsev, O. Inganäs, *Adv. Funct. Mater.* **2006**, *16*, 667; d) Y. Yao, J. Hou, Z. Xu, G. Li, Y. Yang, *Adv. Funct. Mater.* **2008**, *18*, 1783.

[6] R. J. Kline, M. D. McGehee, E. N. Kadnikova, J. Liu, J. M. J. Fréchet, *Adv. Mater.* **2003**, *15*, 1519.

[7] a) C. V. Hoven, X.-D. Dang, R. C. Coffin, J. Peet, T. Q. Nguyen, G. C. Bazan, *Adv. Mater.* **2010**, *22*, E63; b) Z. Li, J. Ding, N. Song, X. Du, J. Zhou, J. Lu, Y. Tao, *Chem. Mater.* **2011**, *23*, 1977.

[8] a) S. Wakim, S. Alem, Z. Li, Y. Zhang, S.-C. Tse, J. Lu, J. Ding, Y. Tao, *J. Mater. Chem.* **2011**, *21*, 10920; b) S. C. Price, A. C. Stuart, W. You, *Macromolecules* **2010**, *43*, 4609; c) R. Qin, W. Li, C. Li, C. Du, C. Veit, H.-F. Schleiermacher, M. Andersson, Z. Bo, Z. Liu, O. Inganäs, U. Wuerfel, F. Zhang, *J. Am. Chem. Soc.* **2009**, *131*, 14612.

[9] a) R. C. Coffin, J. Peet, J. Rogers, G. C. Bazan, *Nat. Chem.* **2009**, *1*, 657; b) Z. H. Li, M. S. Wong, Y. Tao, J. Lu, *Chem. Eur. J.* **2005**, *11*, 3285.

[10] Y. Zhang, J. Zou, H.-L. Yip, Y. Sun, J. A. Davie, K.-S. Chen, O. Acton, A. K.-Y. Jen, *J. Mater. Chem.* **2011**, *21*, 3895.